Journal of Magnetic Resonance **144,** 228–242 (2000)
doi:10.1006/jmre.2000.2055, available online at http://www.idealibrary.com on IDEAL®

Intensity of Cross-Peaks in Hyscore Spectra of $S = 1/2$, $I = 1/2$ Spin Systems

Sergei A. Dikanov,*,†,[1] Alexei M. Tyryshkin,†,‡ and Michael K. Bowman‡

*Illinois EPR Research Center and Department of Veterinary Clinical Medicine, University of Illinois at Urbana–Champaign, Urbana, Illinois 61801; †Institute of Chemical Kinetics and Combustion, Russian Academy of Sciences, Novosibirsk 630090, Russia; and ‡Macromolecular Structure and Dynamics, W. R. Wiley Environmental Molecular Sciences Laboratory, Pacific Northwest National Laboratory, Richland, Washington 99352

Received October 14, 1999; revised February 15, 2000

The cross-peak intensity for a $S = 1/2$, $I = 1/2$ spin system in two-dimensional HYSCORE spectra of single-crystals and powders is analyzed. There is a fundamental difference between these two cases. For single crystals, the cross-peak intensity is distributed between the two (+, +) and (+, −) quadrants of the hyperfine sublevel correlation (HYSCORE) spectrum by the ratio c^2:s^2 (C. Gemperle, G. Aebli, A. Schweiger, and R. R. Ernst, *J. Magn. Reson.* 88, 241 (1990)). However, for powder spectra another factor becomes dominant and governs cross-peak intensities in the two quadrants. This factor is the phase interference between modulation from different orientations of the paramagnetic species. This can lead to essentially complete disappearance of the cross-peak in one of the two (+, +) or (+, −) quadrants. In the (+, +) quadrant, cross-peaks oriented parallel to the main (positive) diagonal of the HYSCORE spectrum are suppressed, while the opposite is true in the (+, −) quadrant where cross-peaks nearly perpendicular to the main (negative) diagonal of HYSCORE spectra are suppressed. Analytical expressions are derived for the cross-peak intensity profiles in powder HYSCORE spectra for both axial and nonaxial hyperfine interactions (HFI). The intensity is a product of two terms, one depending only on experimental parameter (τ) and the other only on the spin Hamiltonian. This separation provides a rapid way to choose τ for maximum cross-peak intensity in a region of interest in the spectrum. For axial HFI, the Hamiltonian-dependent term has only one maximum and decreases to zero at the canonical orientations. For nonaxial HFI, this term produces three separate ridges which outline the whole powder lineshape. These three ridges have the majority of the intensity in the HYSCORE spectrum. The intensity profile of each ridge resembles that observed for axial HFI. Each ridge defines two principal values of the HFI similar to the ridges from an axial HFI. © 2000 Academic Press

Key Words: **pulsed EPR; ESEEM; HYSCORE; lineshape; intensity.**

INTRODUCTION

HYSCORE (hyperfine sublevel correlation) spectroscopy based on the four-pulse two-dimensional (2D) ESEEM experiment (*1*) finds increasing application in the study of complex paramagnetic centers where the unpaired electron interacts with a number of magnetically nonequivalent nuclei (*2–18*). The basic advantage of the HYSCORE technique is the creation of correlation cross-peaks in 2D spectra whose coordinates are nuclear frequencies ($\pm\nu_\alpha$, $\pm\nu_\beta$) from opposite electron spin manifolds (*1, 19*). The cross-peaks significantly simplify analysis of congested spectra by correlating and spreading out the nuclear frequencies.

We have demonstrated that another advantage of orientationally disordered (powder) HYSCORE spectra of $S = 1/2$, $I = 1/2$ spin systems is the visualization of interdependence between ν_α and ν_β belonging to the same orientations in the form of the cross-peak contour projection (*20*). The analysis of the contour allows direct determination of the (electron-nuclear) isotropic and anisotropic hyperfine interactions (HFI) (*12, 20*). However, it is apparent from previous applications of HYSCORE that complete understanding of its spectra does require insight into the cross-peak lineshapes, particularly for nonaxial HFI or when the anisotropy of the EPR spectrum precludes the measurement of a HYSCORE spectrum from all possible orientations of the paramagnetic centers with respect to the magnetic field. One should understand which orientations of the paramagnetic species produce singularities in the 2D spectrum and how the intensity is distributed between the nonequivalent (+, +) and (+, −) quadrants of the 2D spectrum. The present work explores the intensities and shapes of cross-peaks in HYSCORE spectra for $S = 1/2$, $I = 1/2$ and could be extended to $S = 1/2$, $I > 1/2$ systems with negligible nuclear quadrupole interaction.

Both axial and nonaxial HFI are treated. The intensity profile of cross-peaks in the powder spectrum is evaluated and shown to be “bell”-shaped with zero intensity at the canonical HFI orientations and with a single maximum at some intermediate orientation. While nuclear frequencies at canonical orientations are not directly observable, their determination (and subsequent evaluation of complete HFI tensor) is possible from a linear fit of the cross-peak coordinates in a ν_α^2 vs ν_β^2 plot (*20*). In the case of nonaxial HFI, three separate ridges are formed.

[1] To whom correspondence should be addressed. E-mail: dikanov@uiuc.edu.

1090-7807/00 $35.00

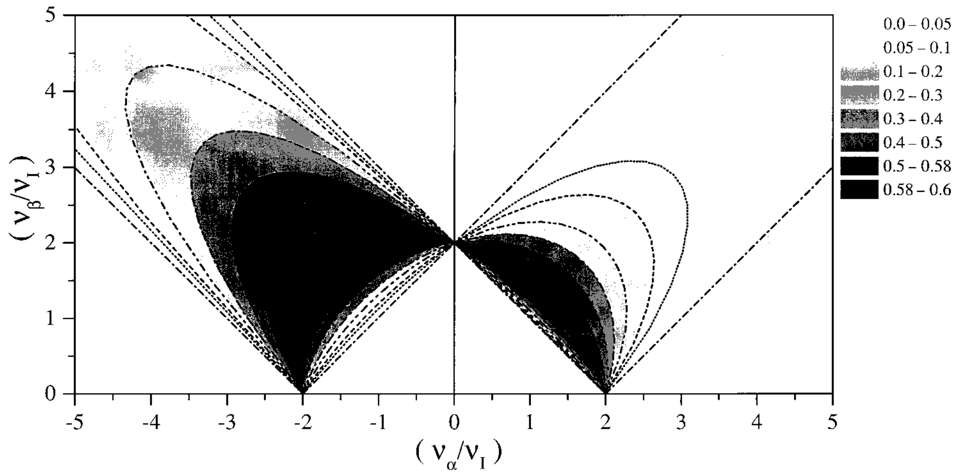

FIG. 1. Contour plot of cross-peak intensity ($I_1^{\pm}$ term) in single-crystal HYSCORE spectrum for $I = 1/2$. The intensity $I_1^{\pm}$ depends only on the dimensionless coordinates (ν_α/ν_I, ν_β/ν_I) of the cross-peak. Positive (ν_α/ν_I) corresponds to the (+, +) quadrant of the spectrum and negative (ν_α/ν_I) to the (+, −) quadrant.

Each ridge indicates two of the three principal values of the HFI in the same manner as the ridges from an axial HFI. These findings provide a basis for rapid interpretation of HYSCORE spectra.

THEORY

Intensity of Cross-Peaks in Single-Crystal HYSCORE Spectra

A cross-peak in the HYSCORE spectra of a $S = 1/2$, $I = 1/2$ electron-nuclear spin system is described in the time domain by (*21*, *22*)

$$V(t_1, t_2) = k \cdot \sin(\pi \nu_\alpha \tau) \cdot \sin(\pi \nu_\beta \tau) \times [c^2 \cos 2\pi(\nu_\alpha t_1 + \nu_\beta t_2 + \nu_+ \tau/2) + c^2 \cos 2\pi(\nu_\alpha t_2 + \nu_\beta t_1 + \nu_+ \tau/2) - s^2 \cos 2\pi(\nu_\alpha t_1 - \nu_\beta t_2 + \nu_- \tau/2) - s^2 \cos 2\pi(\nu_\alpha t_2 - \nu_\beta t_1 + \nu_- \tau/2)] \quad [1]$$

in the limit of complete excitation and nonselective detection, where ν_α and ν_β are the nuclear (positive) frequencies from opposite electron spin manifolds, and $\nu_\pm$ are their linear ($\nu_\alpha \pm \nu_\beta$) combinations; τ, t_1, and t_2 are times between first and second, second and third, and third and forth pulses, respectively. The amplitude coefficient, $k = 4c^2s^2$, is the product of the formally allowed and forbidden EPR transition probabilities, with

$$c^2(s^2) = \frac{|\nu_I^2 - \frac{1}{4}(\nu_\alpha \mp \nu_\beta)^2|}{\nu_\alpha \nu_\beta}, \quad [2]$$

where ν_I is the nuclear Zeeman frequency. In Eq. [2], only those values of ν_α and ν_β are allowed that satisfy the relations $\nu_\alpha + \nu_\beta \geq 2\nu_I$ and $|\nu_\alpha - \nu_\beta| \leq 2\nu_I$, in order to provide meaningful $c^2(s^2) \leq 1$.

The two nuclear frequencies, ν_α and ν_β, may produce four distinct cross-peaks in the HYSCORE spectrum. A pair of peaks ($+\nu_\alpha$, $+\nu_\beta$) and ($+\nu_\beta$, $+\nu_\alpha$) appears in the positive (+, +) quadrant of 2D spectra and another pair ($\pm\nu_{\alpha(\beta)}$, $\mp\nu_{\beta(\alpha)}$) in the other (+, −) quadrant.

The intensity of a cross-peak can be written as

$$I^{\pm}_{\nu_\alpha,\nu_\beta} = k \cdot z^2 \cdot |\sin(\pi \nu_\alpha \tau)\sin(\pi \nu_\beta \tau)|, \quad [3]$$

where z^2 denotes either c^2 for $I^{+}_{\nu_\alpha,\nu_\beta}$ in the (+, +) quadrant or s^2 for $I^{-}_{\nu_\alpha,\nu_\beta}$ in the (+, −) quadrant. The cross-peaks in the (+, +) and (+, −) quadrants also have different phases, $\nu_+\tau/2$ and $\nu_-\tau/2$, respectively. However, HYSCORE spectra are usually represented in absolute Fourier transform mode, which hides the phase information. Therefore, we will not discuss the phases below.

It is convenient to consider the intensity as a product of two terms,

$$I^{\pm}_{\nu_\alpha,\nu_\beta} = I_1^{\pm}(\nu_\alpha/\nu_I,\ \nu_\beta/\nu_I) \cdot I_2(\nu_\alpha \tau,\ \nu_\beta \tau), \quad [4]$$

which are functions of dimensionless variables. The first term, $I_1^{\pm}(\nu_\alpha/\nu_I,\ \nu_\beta/\nu_I) = k \cdot z^2$, describes the underlying intensity and depends only on the two nuclear frequencies (ν_α/ν_I) and (ν_β/ν_I) expressed in terms of the Zeeman frequency. The second, time-dependent term, $I_2(\nu_\alpha \tau,\ \nu_\beta \tau) = |\sin(\pi\nu_\alpha\tau)\sin(\pi\nu_\beta\tau)|$, is responsible for the blind spots in HYSCORE spectra and is a function of the dimensionless parameters $\nu_\alpha \tau$ and $\nu_\beta \tau$. Such a presentation eliminates the influence of the particular type of nucleus (ν_I) and the experimental setup (τ) on the properties of HYSCORE spectra.

The Hamiltonian-dependent term $I_1^{\pm}$ is directly determined-

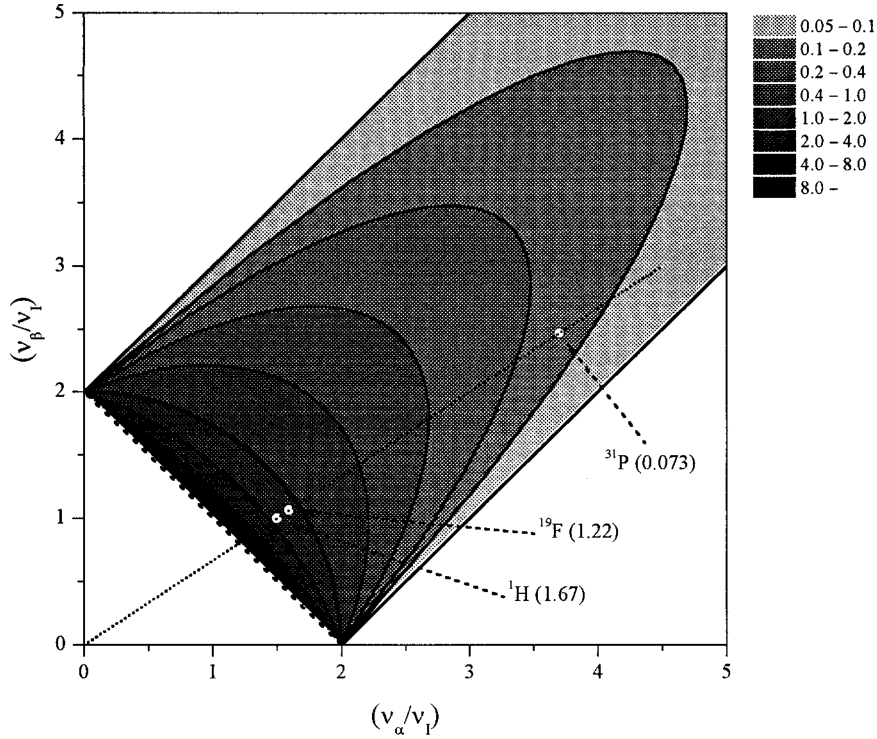

FIG. 2. Ratio I^+/I^- of the cross-peak intensities in the $(+, +)$ and $(+, -)$ quadrants for a single-crystal HYSCORE spectrum of $I = 1/2$ (shown as a contour plot). The bold line represents $(\nu_\alpha/\nu_I, \nu_\beta/\nu_I)$ where intensity of cross-peak is equal in the two quadrants, i.e., $I^+ = I^-$. The open circles lying on the dotted straight line show the location in dimensionless coordinates $(\nu_\alpha/\nu_I, \nu_\beta/\nu_I)$ for the three magnetic nuclei (^{1}H, ^{19}F, ^{31}P) whose actual frequency coordinates (ν_α, ν_β) are coincident (see text). The ratios I^+/I^- are indicated in parentheses for these three nuclei.

by the normalized cross-peak coordinates $(\nu_\alpha/\nu_I, \nu_\beta/\nu_I)$. Figure 1 shows the variation of the cross-peak intensity in the $(+, +)$ and $(+, -)$ quadrants. The maximum intensity of $16/27 \sim 0.6$ occurs for $c^2 = 2/3$ in the $(+, +)$ quadrant and for $c^2 = 1/3$ in $(+, -)$ quadrant. The maximum intensities are observed in a rather narrow range of frequencies. For instance, the peak intensity drops by half in the $(+, +)$ quadrant if either coordinate is greater than 2. When either coordinate becomes >3 the intensity is less than 10%. Reasonable intensities in the $(+, -)$ quadrant are found over a much broader range. The peaks in the $(+, -)$ quadrant reach a maximum intensity with either normalized frequency ~ 2 and the intensity falls off more slowly, dropping by only half for either frequency ~ 3.

This distribution of intensity between $(+, +)$ and $(+, -)$ quadrants is governed by the ratio c^2/s^2 (*21*). Figure 2 shows the calculated ratio, I^+/I^-, in $(\nu_\alpha/\nu_I, \nu_\beta/\nu_I)$ coordinates. I^+/I^- is unity for $c^2 = 1/2$, i.e., $\nu_\alpha^2 + \nu_\beta^2 = 4\nu_I^2$, which is a quarter-circle (bold line in Fig. 2). The cross-peak intensity is greater in the $(+, +)$ quadrant for $\nu_\alpha^2 + \nu_\beta^2 < 4\nu_I^2$, but weaker for $\nu_\alpha^2 + \nu_\beta^2 > 4\nu_I^2$. Thus, a cross-peak with $I^+/I^- > 1$ (or $I^+/I^- < 1$) would indicate a nucleus with $4\nu_I^2$ greater (or less) than $\nu_\alpha^2 + \nu_\beta^2$. This provides a simple method for assigning cross-peaks to a particular type of nucleus according to ν_I. Note that the τ-dependent term I_2 is eliminated in the ratio I^+/I^-, so that the ratio is independent of the experimental conditions. This leads to another useful property of HYSCORE spectra.

If two nuclei of the same isotope but with different hyperfine tensors, for instance, two nonequivalent protons, have accidentally coincident frequencies ($\nu_\alpha^{(1)} = \nu_\alpha^{(2)}$ and $\nu_\beta^{(1)} = \nu_\beta^{(2)}$), then their cross-peak intensity ratios will be equal, $I^+/I^-(\nu_\alpha^{(1)}, \nu_\beta^{(1)}) = I^+/I^-(\nu_\alpha^{(2)}, \nu_\beta^{(2)})$. This is true regardless of the actual hyperfine tensors or the number of equivalent nuclei as long as the pairs of frequencies coincide. On the other hand, if two different isotopes (for instance, ^{1}H and ^{31}P or ^{19}F) have identical frequencies, $\nu_\alpha^{(H)} = \nu_\alpha^{(P)}$ and $\nu_\beta^{(H)} = \nu_\beta^{(P)}$, the cross-peak intensity ratios will differ, $I^+/I^-(\nu_\alpha^{(H)}, \nu_\beta^{(H)}) \neq I^+/I^-(\nu_\alpha^{(P)}, \nu_\beta^{(P)})$. This is because the cross-peaks, when scaled by the different nuclear Zeeman frequencies, map to different coordinates on the dimensionless plots $(\nu_\alpha/\nu_I, \nu_\beta/\nu_I)$. This property is potentially useful for assigning a cross-peak whose origin is ambiguous. One can measure the intensity ratio I^+/I^- of the cross-peak in the $(+, +)$ and $(+, -)$ quadrants in an experimental spectrum and correlate that ratio to the dimensionless plot of I^+/I^- in Fig. 2. For instance, $\nu_\alpha^{(H)} = \nu_\alpha^{(F)} = \nu_\alpha^{(P)} = 22.35$ MHz and $\nu_\beta^{(H)} = \nu_\beta^{(F)} = \nu_\beta^{(P)} = 14.9$ MHz will map to the filled circles on Fig. 2 and give a ratio $I^+/I^- = 1.67$ for ^{1}H ($\nu_I = 14.9$ MHz at 350 mT), $I^+/I^- = 1.22$ for ^{19}F ($\nu_I = 14.03$ MHz), and $I^+/I^- = 0.073$ for ^{31}P ($\nu_I = 6.04$ MHz), which are sufficiently different to identify the nucleus.

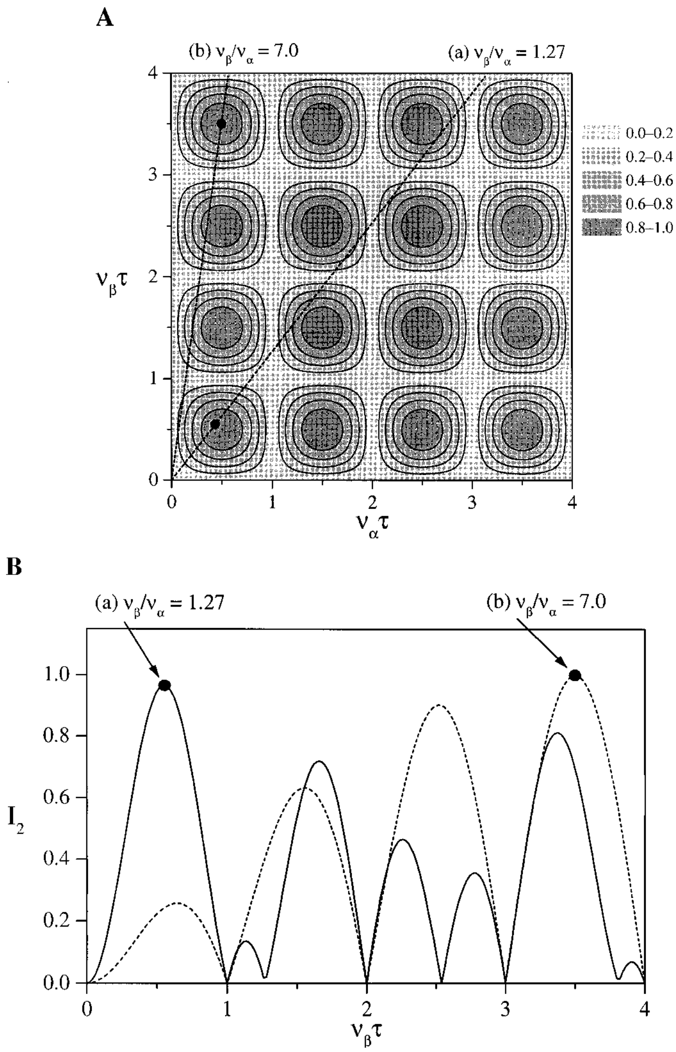

FIG. 3. The τ-suppression effect in HYSCORE: (A) Contour plot of I_2 in dimensionless coordinates ($\nu_\alpha\tau$, $\nu_\beta\tau$). (B) Intensity profile I_2 along the dashed lines on plot (A) which correspond to cross-peaks with $\nu_\beta/\nu_\alpha = 7.0$ and 1.27. Solid circles indicate a choice of optimal τ for maximum cross-peak intensity.

Figure 3A displays the second, time-dependent term, $I_2(\nu_\alpha\tau, \nu_\beta\tau)$, as a function of $\nu_\alpha\tau$ and $\nu_\beta\tau$. When either $\nu_\alpha\tau$ or $\nu_\beta\tau$ equals an integer value, the cross-peak intensity falls to zero, an effect known as a blind-spot (*23*). The time, τ, is an adjustable parameter in a HYSCORE experiment, and values of τ corresponding to intensity maxima or minima for a peak at (ν_α, ν_β) can be found from Fig. 3A. A straight line through the origin with a slope equal to ν_α/ν_β traces out the relative cross-peak intensity as a function of τ. If the difference between the frequencies is small so that their ratio is near unity, the maximum cross-peak intensity occurs close to the first maximum of $I_2(\nu_\alpha\tau, \nu_\beta\tau)$ at $\nu_\alpha\tau = \nu_\beta\tau = 0.5$. As the difference between frequencies increases and their ratio deviates from unity, the τ providing the maximum cross-peak intensity increases. Two examples of this strategy are presented in Fig. 3B. Here the intensity profiles of I_2 are shown along the dashed lines "a, b" of Fig. 3A. For $\nu_\alpha/\nu_\beta = 1.27$ (a), the maximum intensity $I_2 = 0.97$ is achieved at ($\nu_\alpha\tau = 0.43$, $\nu_\beta\tau = 0.55$), or $\nu_I\tau \cong 0.5$. However, for a cross-peak with significantly different frequencies and a higher ratio $\nu_\alpha/\nu_\beta = 7$ (b), one would use a larger τ corresponding to the third or fourth maximum of I_2, ($\nu_\alpha\tau = 0.36$, $\nu_\beta\tau = 2.5$) or ($\nu_\alpha\tau = 0.5$, $\nu_\beta\tau = 3.5$).

Intensity of Cross-Peaks from Axial HFI in Powder HYSCORE Spectra

For orientationally disordered samples, expression [1] must be integrated over the different orientations of the paramagnetic species. For axial HFI, the orientation is defined by a single angle θ, relating the applied magnetic field direction to the principal axis of the HFI tensor. Writing the nuclear frequencies in the form

$$\nu^2_{\alpha(\beta)} = (\nu^2_{\|\alpha(\beta)} - \nu^2_{\perp\alpha(\beta)}) \cdot \cos^2\theta + \nu^2_{\perp\alpha(\beta)} \qquad [5]$$

emphasizes the unique mapping between $\nu_{\alpha(\beta)}$ and θ. Here, $\nu_{\|\alpha(\beta)} = |-\nu_I \pm (a + 2T)/2|$ and $\nu_{\perp\alpha(\beta)} = |-\nu_I \pm (a - T)/2|$ are the nuclear frequencies at the canonical orientations ($\theta = 0$ or $\pi/2$) with the HFI described by its isotropic component (a) and anisotropic tensor ($-T$, $-T$, $2T$). In powder spectra, the two nuclear frequencies $\nu_{\alpha(\beta)}$ vary in a correlated manner over the entire interval between $\nu_{\|\alpha(\beta)}$ and $\nu_{\perp\alpha(\beta)}$. The one-to-one mapping of $\nu_{\alpha(\beta)}$ to θ in Eq. [5] produces a unique mapping between ν_α and ν_β (*20*):

$$\nu^2_{\alpha(\beta)} = Q_{\alpha(\beta)}\nu^2_{\beta(\alpha)} + G_{\alpha(\beta)}, \qquad [6]$$

with $Q_{\alpha(\beta)} = (T + 2a \mp 4\nu_I)/(T + 2a \pm 4\nu_I)$ and $G_{\alpha(\beta)} = \pm 2\nu_I(4\nu_I^2 - a^2 + 2T^2 - aT)/(T + 2a \pm 4\nu_I)$, defining the footprint or contour lineshape of the cross-peak in the 2D spectrum. Equation [6] shows that the cross-peak contour forms a smooth arc in powder 2D spectra between ($|\nu_{\|\alpha(\beta)}|$, $|\nu_{\|\beta(\alpha)}|$) and ($|\nu_{\perp\alpha(\beta)}|$, $|\nu_{\perp\beta(\alpha)}|$). If $Q_{\alpha(\beta)} < 0$, the contour is a portion of an ellipse (circle if $Q_{\alpha(\beta)} = -1$) with its origin at (0, 0). If $Q_{\alpha(\beta)} > 0$, the contour is a hyperbolic segment. When plotted against coordinates ν_α^2 and ν_β^2, the contours become straight-line segments whose slope and intercept allow direct estimation of $Q_{\alpha(\beta)}$ and $G_{\alpha(\beta)}$ and subsequently the isotropic (a) and anisotropic (T) HFI parameters (*12, 20*). Alternatively, the points where the straight-line segment intersects the curve $|\nu_\alpha \pm \nu_\beta| = 2\nu_I$ are ($|\nu_{\|\alpha(\beta)}|$, $|\nu_{\|\beta(\alpha)}|$) and ($|\nu_{\perp\alpha(\beta)}|$, $|\nu_{\perp\beta(\alpha)}|$), from which one can determine the hyperfine tensor (*12*).

Our aim is now to describe the variation of intensity along the contour arc. We start with the relation between the spectral density S_{ν_α,ν_β} and the angular intensity distribution $I(\theta)$ in a random powder:

$$S_{\nu_\alpha,\nu_\beta} \cdot d\nu_c = I(\theta) \cdot \sin\theta \cdot d\theta,$$

or, equivalently, $S_{\nu_\alpha,\nu_\beta} = I(\theta) \cdot \sin\theta \cdot |d\theta/d\nu_c|$, where $d\nu_c =$

$d\theta \cdot [(d\nu_\alpha/d\theta)^2 + (d\nu_\beta/d\theta)^2]^{1/2}$ is an element of the cross-peak arc. $I(\theta) = I^{\pm}_{\nu_\alpha,\nu_\beta}(\theta)$ is the cross-peak intensity from Eq. [4] with the explicit dependence on orientation θ, and $\sin\theta$ is the statistical factor that accounts for the fact that more orientations have $\theta \sim \pi/2$ than $\theta \sim 0$. Calculating the derivative,

$$|d\nu_{\alpha(\beta)}/d\theta| = |\nu^2_{\|\alpha(\beta)} - \nu^2_{\perp\alpha(\beta)}|\sin\theta\cos\theta/\nu_{\alpha(\beta)},$$

one obtains

$$\sin\theta \cdot |d\theta/d\nu_c| = \frac{\nu_\alpha\nu_\beta}{\cos\theta \cdot \sqrt{(\nu^2_{\|\alpha} - \nu^2_{\perp\alpha})^2 \cdot \nu^2_\beta + (\nu^2_{\|\beta} - \nu^2_{\perp\beta})^2 \cdot \nu^2_\alpha}}.$$

Using $\nu_{\|\alpha(\beta)} - \nu_{\perp\alpha(\beta)} = \pm 3/2\ T$, the intensity profile of the powder cross-peak becomes

$$S^{\pm}_{\nu_\alpha,\nu_\beta} = I^{\pm}_1(\nu_\alpha/\nu_I,\ \nu_\beta/\nu_I) \cdot I_2(\nu_\alpha\tau,\ \nu_\beta\tau) \times I_3(\nu_\alpha,\nu_\beta|\nu_I,\ a,\ T), \quad [7]$$

where an additional term appears compared to the single-crystal result [4]:

$$I_3(\nu_\alpha,\ \nu_\beta;\ \nu_I,\ a,\ T) = \frac{\nu_\alpha\nu_\beta}{3/2|T| \cdot \cos\theta \cdot \sqrt{(\nu_{\|\alpha} + \nu_{\perp\alpha})^2 \cdot \nu^2_\beta + (\nu_{\|\beta} + \nu_{\perp\beta})^2 \cdot \nu^2_\alpha}}. \quad [8]$$

Equations [7] and [8] describe the intensity at (ν_α, ν_β) along the top of the powder cross-peak ridge produced by the HFI [6]. The term I_3 has singularities for $\cos\theta = 0$ and $T = 0$ which are never observable because they occur where $I^{\pm}_1 = 0$.

To eliminate the apparent singularities of I_3, we rewrite Eq. [7] in the following form:

$$S^{\pm}_{\nu_\alpha,\nu_\beta} = I^{\pm}_{13}(\nu_\alpha,\ \nu_\beta;\ \nu_I,\ a,\ T) \cdot I_2(\nu_\alpha\tau,\ \nu_\beta\tau), \quad [9]$$

with

$$I^{\pm}_{13}(\nu_\alpha,\ \nu_\beta;\ \nu_I,\ a,\ T) \equiv I^{\pm}_1 \cdot I_3 = \frac{6|T| \cdot \nu^2_I z^2 \cos\theta \cdot \sin^2\theta}{\nu_\alpha\nu_\beta\sqrt{(\nu_{\|\alpha} + \nu_{\perp\alpha})^2\nu^2_\beta + (\nu_{\|\beta} + \nu_{\perp\beta})^2\nu^2_\alpha}}, \quad [10]$$

and $z^2 \equiv c^2(s^2)$ defined in Eq. [2]. The product $I^{\pm}_{13}$ describes the "blind-spot-free" intensity of the powder cross-peak. Numerical simulations show that for all reasonable sets of HFI parameters ($|a/\nu_I| \leq 5$, $|T/\nu_I| \leq 5$) the cross-peaks have a smooth shape with a single maximum and intensity decreasing to zero at the canonical orientations (see examples on Figs. 8A and 8B). Such a bell shape is easily understood as determined mainly by the numerator term $\cos\theta \cdot \sin^2\theta$ in Eq. [10].

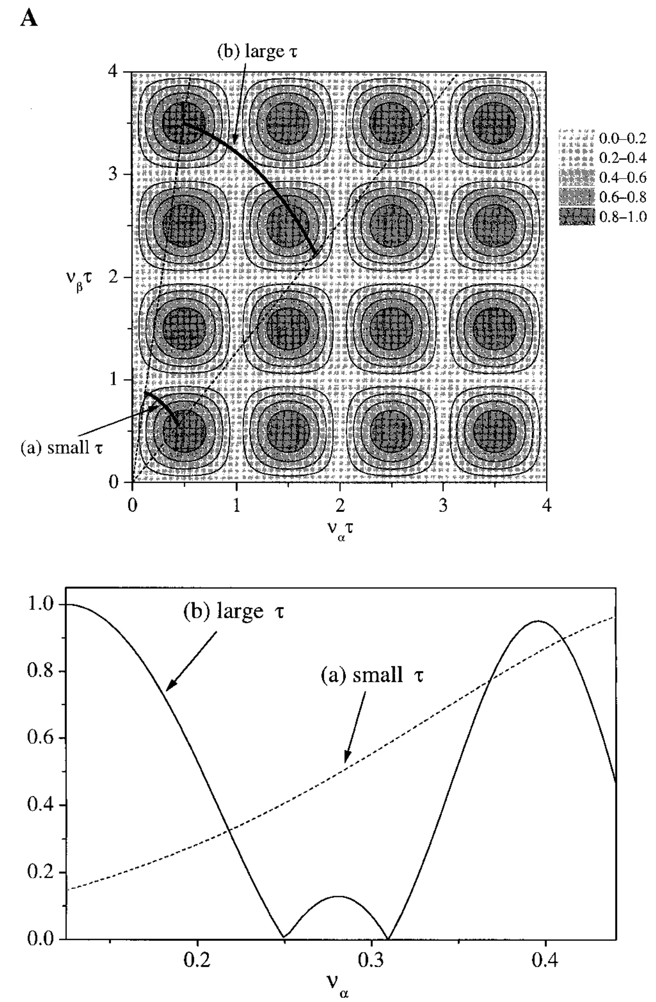

FIG. 4. The τ-suppression effect in powder HYSCORE: (A) A powder arc ridge of the same arbitrary cross-peak is schematically represented (bold lines) for small and large τ values on a contour plot of I_2 in dimensionless coordinate $(\nu_\alpha\tau,\ \nu_\beta\tau)$. (B) Intensity profile I_2 along the powder cross-peak ridge for small and large τ.

It is difficult to optimize τ for maximum intensity $I_2(\tau)$ along the entire powder cross-peak. The variation of I_2 along a cross-peak ridge for an arbitrary HFI is illustrated in Fig. 4A, where the same cross-peak is scaled for small (a) and large (b) values of τ. The two values are chosen for maximum intensity at the right or left end of the powder cross-peak. Figure 4B shows the intensity profile of I_2 along the two ridges (a) and (b). The larger τ_b produces a very distorted shape with cross-peak intensity completely suppressed at two different points. On the other hand, much of the intensity is lost near one of the edges of the cross-peak for the smaller τ_a. This example demonstrates the necessity for 2D experiments to use several distinct τ to enhance different regions of the extended powder cross-peak. Cross-peaks from spectra at different τ can be assigned to the same HFI by overlaying spectra plotted in ν_α^2 vs ν_β^2 coordinates (*12*). This procedure reconstructs the blind-spot-free contour. The optimal τ for any particular point along the powder cross-peak remains the same as for single-crystal HYSCORE spectra (Fig. 3).

Our final step, however, is to analyze how the practicalities of data collection modify the features of HYSCORE spectra that are formulated above.

Interference Effects in Powder HYSCORE Spectra

HYSCORE spectra are obtained by absolute mode Fourier transformation of experimentally collected time-domain data. Interference effects are often encountered when experimental observables are derived in such a fashion. An example very close to this subject is the spin-echo phenomenon. Spin packets, precessing at different frequencies owing to inhomogeneous broadening, yield an observable signal, either immediately after a single excitation pulse in the form of an FID or as an echo when their phases are "refocused" by additional pulses. There is no observable signal at all other times, because each spin packet precesses with its own frequency, and the total magnetization from the ensemble of spin packets with different phases is vanishingly small on account of their interference. It has not been widely appreciated that signals from paramagnetic species with different orientations can interfere with each other in powder HYSCORE and alter the observed spectral intensity.

Equation [1] for 2D HYSCORE of an $I = 1/2$ nucleus can be conveniently rewritten in the form

$$\begin{aligned} V(t_1, t_2) \propto \langle c^2 \cdot (&e^{-i\cdot 2\pi(\nu_\alpha t_1 + \nu_\beta t_2 + (\nu_\alpha+\nu_\beta)\tau/2)} \\ &+ e^{-i\cdot 2\pi(\nu_\alpha t_2 + \nu_\beta t_1 + (\nu_\alpha+\nu_\beta)\tau/2)} + \text{c.c.}) \\ - s^2 \cdot (&e^{-i\cdot 2\pi(\nu_\alpha t_1 - \nu_\beta t_2 + (\nu_\alpha-\nu_\beta)\tau/2)} \\ &+ e^{-i\cdot 2\pi(\nu_\alpha t_2 - \nu_\beta t_1 + (\nu_\alpha-\nu_\beta)\tau/2)} + \text{c.c.})\rangle_\Omega, \end{aligned} \quad [11]$$

where c.c. indicates the complex conjugate of the previous terms, and $\langle .. \rangle_\Omega$ the powder average over different orientations Ω of the external magnetic field. One can consider only the first term $e^{-i\cdot 2\pi(\nu_\alpha t_1 + \nu_\beta t_2 + (\nu_\alpha + \nu_\beta)\tau/2)}$ of Eq. [11] without loss of generality, because each term produces a distinct peak that nevertheless is subject to similar considerations.

The first term corresponds to cross-peak $(+\nu_\alpha, +\nu_\beta)$. Both $\nu_{\alpha(\beta)}(\Omega)$ vary on Ω producing an extended cross-peak ridge in the powder spectrum whose profile is described by Eq. [6]. Importantly, not only the magnitude c^2 but also the phase

$$\begin{aligned} \text{ph}(\Omega, t_1, t_2) = \nu_\alpha(\Omega)t_1 + \nu_\beta(\Omega)t_2 \\ + (\nu_\alpha(\Omega) + \nu_\beta(\Omega))\tau/2 \end{aligned} \quad [12]$$

varies for each set of $(\nu_\alpha(\Omega), \nu_\beta(\Omega))$. Because of different phases, the spin packets Ω summed at the time point (t_1, t_2) destructively interfere with each other in the sum $\langle c^2 \cdot e^{-i\cdot 2\pi(\nu_\alpha t_1 + \nu_\beta t_2 + (\nu_\alpha + \nu_\beta)\tau/2)}\rangle_\Omega$. It will be shown below that modulation intensity in the time domain vanishes except at (t_1, t_2) points where spin packets arrive with essentially the same phase, i.e., $\text{ph}(\Omega, t_1, t_2) \equiv \text{ph}(t_1, t_2)$ independent on Ω. At these time points, the packets are accumulated "in-phase" and produce the maximum modulation amplitude for $\langle c^2 \cdot e^{-i\cdot 2\pi(\nu_\alpha t_1 + \nu_\beta t_2 + (\nu_\alpha + \nu_\beta)\tau/2)}\rangle_\Omega$.

For simplicity, we shall assume a local linear relationship between ν_α and ν_β at every orientation Ω. That is, we expand ν_α as a Taylor series in ν_β and retain only the leading terms:

$$\nu_\alpha(\Omega) = b_1 \cdot \nu_\beta(\Omega) + b_0. \quad [13]$$

This assumption is allowed because the powder cross-peak ridge is only weakly curved [6]. Substitution of [13] into [12] gives

$$\begin{aligned} \nu_\beta(\Omega) \cdot [b_1 t_1 + t_2 + (b_1 + 1)\tau/2] \\ + b_0(t_1 + \tau/2) \equiv \text{ph}(t_1, t_2), \end{aligned}$$

which is true for all $\nu_\beta(\Omega)$ when

$$b_1 t_1 + t_2 + (b_1 + 1)\tau/2 = 0. \quad [14]$$

Equations [13] and [14] establish the relationship between the frequency domain and time domain in the powder HYSCORE spectra. Each linear segment [13] of a cross-peak in the "ideal" frequency domain produces a signal along a straight line [14] in the time domain.

Figure 5 illustrates this consideration. Here "idealized" 2D spectra (left) are constructed from a segment of the powder cross-peak (ν_α, ν_β) approximated by a straight line [13] (the coefficients b_1 and b_0 are in the figure legend). The mirror cross-peaks (ν_β, ν_α) and $(-\nu_{\alpha(\beta)}, -\nu_{\beta(\alpha)})$ corresponding to the other terms of Eq. [11] are also added. On the right side of Fig. 5, the corresponding idealized time domains are shown calculated by the inverse Fourier transformation. The time-domain intensity is concentrated along two crossed lines. One of these lines is described by [14], and the second line corresponds to the exchange of t_1 and t_2:

$$b_1 t_2 + t_1 + (b_1 + 1)\tau/2 = 0 \quad [15]$$

from the mirror cross-peak (ν_β, ν_α). The signal is rapidly attenuated away from the lines [14, 15]. The more distant a (t_1, t_2)-point from the lines, the stronger the suppression. Quantitatively, the width of the in-phase lines in the time domain is inversely related to the length of the cross-peak in the frequency spectrum $\sim 1/[(\nu_{\alpha\perp} - \nu_{\alpha\|})^2 + (\nu_{\beta\perp} - \nu_{\beta\|})^2]^{1/2}$. The modulation intensity decays along the in-phase lines as the

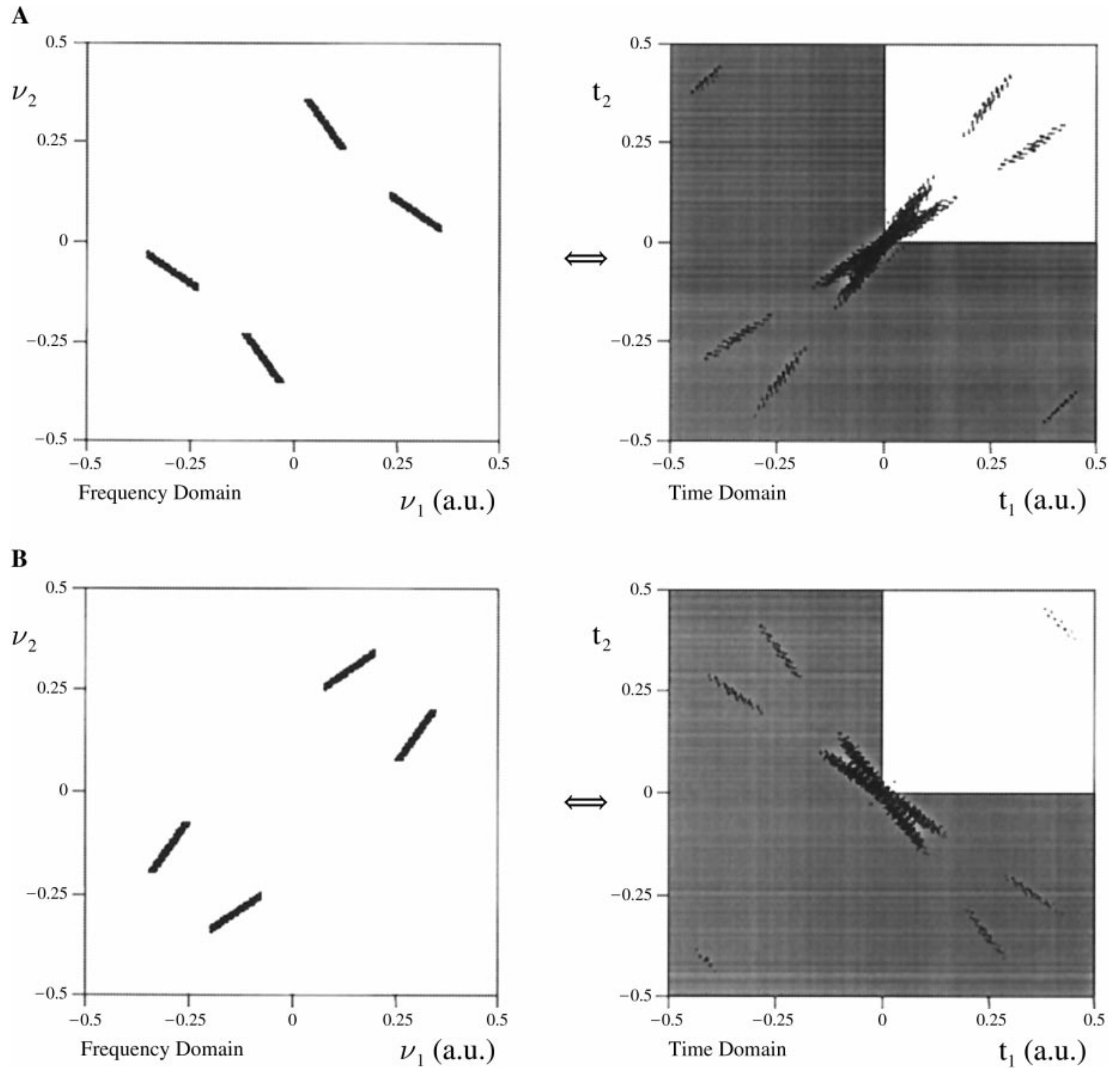

FIG. 5. Interference effects in the powder HYSCORE. The time-domain plots (right side of each pair) were obtained by direct inverse Fourier transformation of the corresponding frequency-domain spectra (left). Only the light area ($+t_1$, $+t_2$) in the time domain is measurable in the experiment. (A–D) Four different situations for powder cross-peaks in the 2D spectrum (see Eq. [13]): (A) (b_0, b_1) = (+0.27, −0.7), (B) (+0.2, +0.7), (C) (+0.41, −0.7), (D) (+0.22, +0.3).

inverse of the cross-peak width in the spectrum. Thus, to recover the idealized spectrum, it is necessary and sufficient to measure just the lines in the time domain.

The four pairs of frequency and time-domains shown in Fig. 5 represent the four different powder cross-peak orientations which are typical in a 2D spectra (*2–19*). In Fig. 5A, the cross-peaks are located in the (+, +) and (−, −) quadrants and their orientation is roughly perpendicular to the main (positive) diagonal of the 2D spectrum ($b_1 < 0$). The corresponding time-domain signal (Fig. 5A, right) appears in the ($+t_1$, $+t_2$) and ($-t_1$, $-t_2$) quadrants as two lines in accordance with Eqs. [14] and [15]. In Fig. 5B, the cross-peaks are still in the (+, +) and (−, −) quadrants but now are nearly parallel to the main diagonal ($b_1 > 0$). The change of orientation leads to a relocation of the straight lines to the ($\pm t_1$, $\mp t_2$) quadrants in the time domain. The idealized time domains in Fig. 5 extend over both positive and negative times $t_{1(2)}$. However, only the upper right quadrant of the time-domain pattern, ($t_1 > 0$, $t_2 > 0$), has a physical meaning and is measurable in an experiment. The other three quadrants (shaded in Fig. 5) are eternally inaccessible. It becomes clear that cross-peaks of nearly parallel orientation (Fig. 5B) should be strongly suppressed in real spectra because their signals fall predominantly in the unmeasurable ($\pm t_1$, $\mp t_2$) quadrants, and only shallow traces leak into

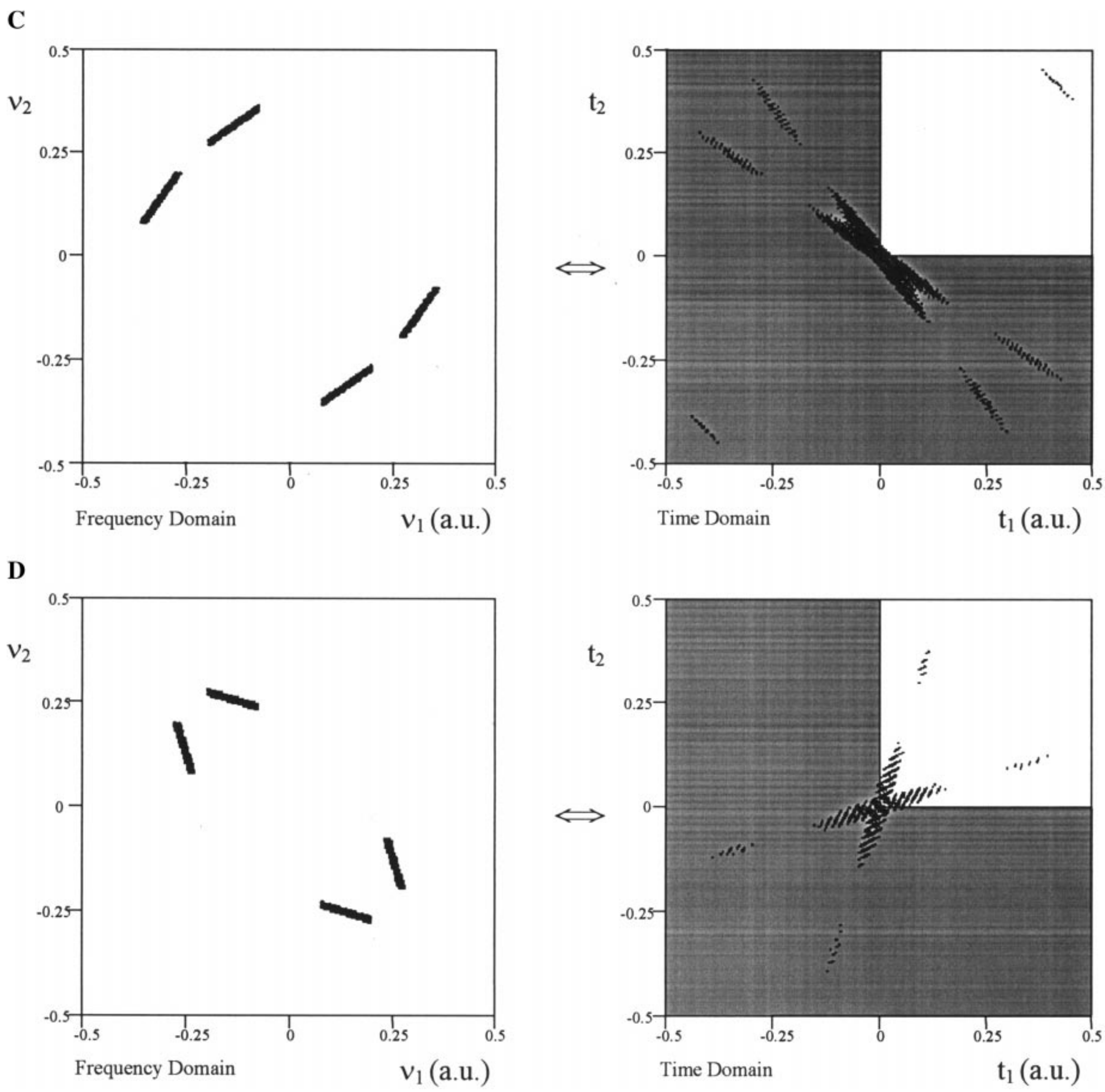

FIG. 5—*Continued*

the $(+t_1, +t_2)$ quadrant. On the other hand, cross-peaks with perpendicular orientation (Fig. 5A) are readily detectable.

Opposite results are found for cross-peaks in the $(\pm, \mp)$ quadrants of the 2D spectra (Figs. 5C and 5D). Considering the term $\langle e^{-i\cdot 2\pi(\nu_\alpha t_1 - \nu_\beta t_2 + (\nu_\alpha - \nu_\beta)\tau/2)}\rangle_\Omega$ and taking the same linear relationship [13] between $\nu_{\alpha(\beta)}$ frequencies, one arrives at two straight lines in the time domain:

$$b_1 t_1 - t_2 + (b_1 - 1)\tau/2 = 0,$$
$$b_1 t_2 - t_1 + (b_1 - 1)\tau/2 = 0. \qquad [16]$$

In contrast to the $(\pm, \pm)$ cross-peaks considered above, now the $b_1 > 0$ orientations dominate experimental spectra, and $b_1 < 0$ cross-peaks are suppressed (Figs. 5C and 5D). The influence of interference on cross-peak intensity in powder HYSCORE spectra is summarized in Table 1.

Generalization of the straight-line approximation to the real cross-peak shapes [6] is straightforward. Since each cross-peak is a smooth arc, every local segment can be approximated piecewise by a linear relation with slope $b_1(\theta)$:

$$b_1(\theta) = \frac{d\nu_\alpha}{d\nu_\beta}(\theta) = Q_\alpha \cdot \nu_\beta/\nu_\alpha.$$

The frequencies $\nu_{\alpha(\beta)}$ are by convention positive values, there-

TABLE 1
Influence of Powder Interference Effects on Cross-Peak Appearance in 2D HYSCORE Spectra

Cross-peak allocation	$b_1 > 0$ ($Q_\alpha > 0$)	$b_1 < 0$ ($Q_\alpha < 0$)	$b_1 \approx 0$ or $b_1 \to \infty$
(+, +) Quadrant	Suppressed	Allowed	Strongly affected
(+, −) Quadrant	Allowed	Suppressed	Strongly affected

fore the sign of $b_1(\theta)$ is solely determined by the term $Q_\alpha = (T + 2a - 4\nu_I)/(T + 2a + 4\nu_I)$. Although the magnitude varies, $b_1(\theta)$ retains its sign along the entire cross-peak, from $\theta = 0$ to $\pi/2$. Hence, Q_α is the only parameter that determines cross-peak appearance in a 2D spectrum. Figure 6A shows the regions of $Q_\alpha > 0$ and $Q_\alpha < 0$ in the coordinates $(T/\nu_I, a/\nu_I)$. For the crosshatched region, $Q_\alpha < 0$ and hence $b_1(\theta) < 0$ for all the $(\Delta\theta)_\theta$-segments of the entire cross-peak. In accordance with Table 1, each $(\Delta\theta)_\theta$-segment and thus the entire cross-peak produced by the nucleus with hyperfine parameters from this region will be observed in the (+, +) quadrant and supressed in (+, −). For HFI parameters from the dotted regions, $Q_\alpha > 0$ and $b_1(\theta) > 0$, and the cross-peak behaves in the opposite fashion. Figure 6B shows a similar plot for single-crystal HYSCORE spectra where the intensity is distributed according to the $c^2{:}s^2$ rule: for smaller hyperfine interactions the greater intensity is found in the (+, +) quadrant but for larger interactions the intensity found in the (+, −) quadrant. While the $c^2{:}s^2$ ratio is still relevant in the powder case, interference effects become the dominating factor and can completely suppress the cross-peak intensity in one of the (+, +) or (+, −) quadrants, regardless of the actual $c^2{:}s^2$ ratio.

Figure 7A presents a single-crystal HYSCORE spectrum calculated for $\nu_I = 1$ MHz, $a = 2$ MHz, $T = -2$ MHz, and $\theta = 65°$ (the parameters are marked with solid circles in Figs. 6A and 6B). As predicted, the ratio $I^+ < I^-$ is observed in the spectrum, following the theoretical $c^2{:}s^2 = 0.256$. Single-crystal simulations for other orientations θ followed the same relationship $I^+ < I^-$. The powder spectrum simulated with the same parameters (Fig. 7B) has, however, the opposite intensity ratio $I^+ > I^-$. The intensity I^- vanishes in powder spectrum due to interference, and only a few weak features can be discovered.

We have not been able to explicitly derive the interference term I_4 that would describe the cross-peak intensity in

$$S^{\pm}_{\nu_\alpha,\nu_\beta} = I^{\pm}_{13}(\nu_\alpha,\ \nu_\beta;\ \nu_I,\ a,\ T) \cdot I_2(\nu_\alpha\tau,\ \nu_\beta\tau) \cdot I_4(Q_{\alpha(\beta)}). \quad [17]$$

However, interference effects can be approximated by a step function, equal to 1 or 0 depending on the sign of $Q_{\alpha(\beta)}$:

$$I_4(Q_{\alpha(\beta)}) = \begin{cases} 1 & (+,+) \text{ cross-peak with } Q_{\alpha(\beta)} < 0, \quad \text{and} \\ & (+,-) \text{ cross-peak with } Q_{\alpha(\beta)} > 0 \\ 0 & (+,+) \text{ cross-peak with } Q_{\alpha(\beta)} > 0, \quad \text{and} \\ & (+,-) \text{ cross-peak with } Q_{\alpha(\beta)} < 0. \end{cases} \quad [18]$$

This completely suppresses the cross-peak intensity in one quadrant $(I_4(Q_\alpha) = 0)$ but leaves the intensity unaffected in the other $(I_4(Q_\alpha) = 1)$. Simulations in Fig. 8 illustrate the approximation. The cross-peak intensity (solid) taken as a skyline projection of simulated HYSCORE spectra is com-

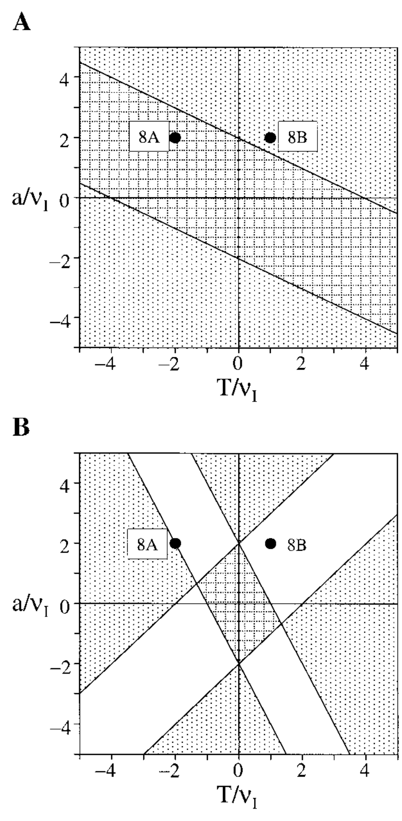

FIG. 6. (A) Graphic presentation of the cross-peak appearance in powder HYSCORE spectra ("$Q_\alpha > 0$ and $Q_\alpha < 0$" rule). For the parameters $(T/\nu_I, a/\nu_I)$ of the central (crosshatched) region ($Q_\alpha < 0$), the cross-peak is only detected in the (+, +) quadrant, and for the parameters of the dotted regions ($Q_\alpha > 0$) the cross-peak intensity is only observed in the (+, −) quadrant. (B) Graphic presentation of the cross-peak intensity allocation in single-crystal HYSCORE spectrum ("$c^2{:}s^2$" rule). For hyperfine parameters $(T/\nu_I, a/\nu_I)$ in the central (crosshatched) region, the most cross-peak intensity lies in the (+, +) quadrant of 2D spectra, i.e., $I^+ > I^-$ for any orientation θ of the axial HFI tensor relative to the external magnetic field. The reverse ($I^+ < I^-$) is true for hyperfine parameters in the dotted regions. Unmarked regions represent the parameters for which ratio of the cross-peak intensity in the (+, +) or (+, −) quadrant varies with θ. The parameters used in the simulations of Figs. 7, 8A, and 8B are marked with solid circles on the graphs.

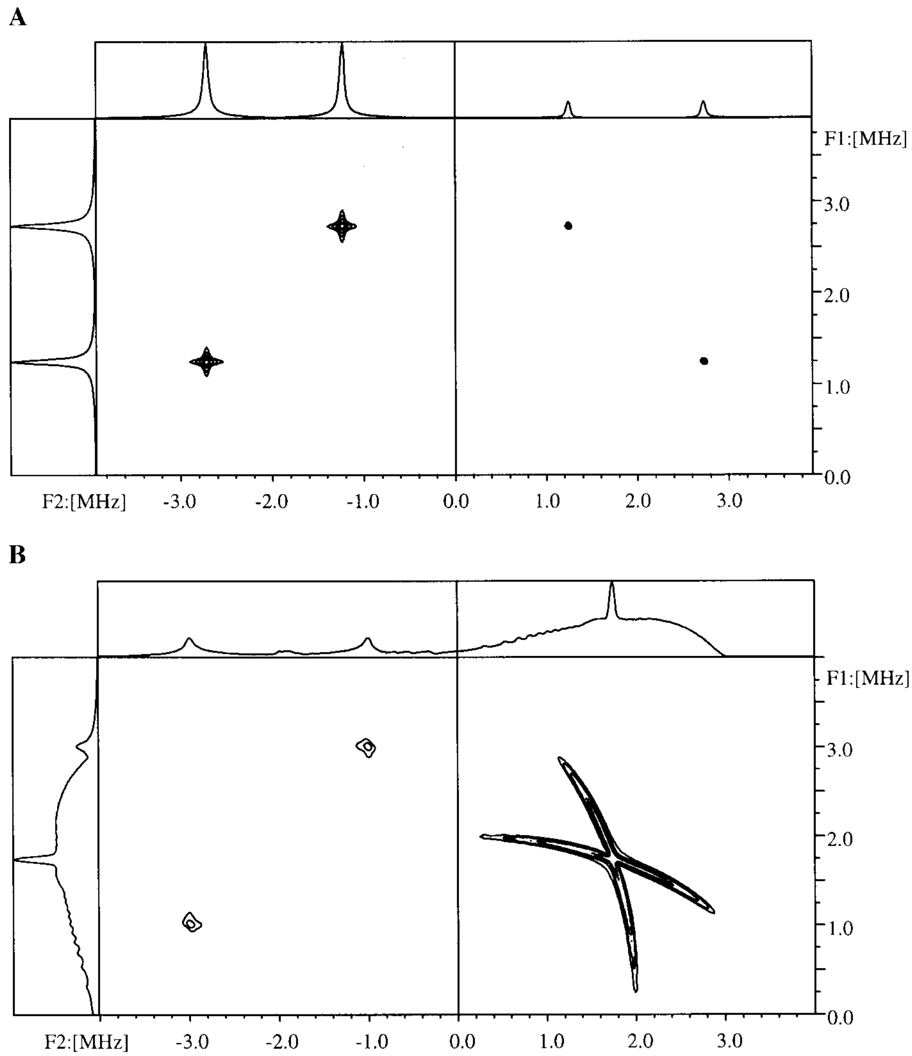

FIG. 7. Single-crystal (A) and powder (B) HYSCORE spectra from an $I = 1/2$ nucleus with the hyperfine parameters ($\nu_I = 1$ MHz, $a = 2$ MHz, $T = -2$ MHz) marked with solid circles on the graphs in Figs. 6A and 6B. An orientation, $\theta = 65°$, for the axial HFI tensor relative to the external magnetic field is assumed in the single-crystal simulation.

pared to the idealized interference-free intensity predicted with [10] (dashed lines). The intensities I^+ in Fig. 8A and I^- in Fig. 8B are well reproduced, so that $I_4(Q_\alpha) = 1$ would be a good approximation. But only a few weak features are seen in the region of the strongly suppressed lines in the opposite quadrants, I^- in Fig. 8A and I^+ in Fig. 8B. These features correspond to nuclear frequencies $\nu_{\perp\alpha(\beta)}$ near the perpendicular orientation of the magnetic field, which are the only ones remaining from the entire powder cross-peak. The effect resembles that described for the dead time distortion of the powder lineshapes in 1D ESEEM spectra (*24*).

Two special cases, $b_1 \approx 0$ and $b_1 \rightarrow \infty$, mark the boundaries in the approximation [18]. These are known as the S-singularity in 1D ESEEM spectroscopy where $|\nu_{\|\alpha(\beta)}| = |\nu_{\perp\alpha(\beta)}|$ and either ν_α or ν_β is orientation independent. With $b_1 \approx 0$ ($b_1 \rightarrow \infty$), one of the lines [14], [15], or [16] in the time domain lies nearly on the t_1 axis and the other on the t_2 axis. Considering that the $(+t_1, +t_2)$ quadrant is the only one observable in the experiment, it becomes clear that the cross-peak intensity in both the $(+, +)$ and the $(+, -)$ quadrants will be affected near these special cases. For finite τ, the pairs of lines [14], [15], or [16] intersect at negative times ($t_1 = -\tau/2$, $t_2 = -\tau/2$), Fig. 9, and the measurable portion of signal in the $(+t_1, +t_2)$ quadrant is partially or totally lost. One can think of the τ-shift as an additional dead time ($t_{dead} = \tau/2$) in both dimensions.

Interference is not specific to the $S = 1/2$, $I = 1/2$ system but is a general feature of 2D spectra from nuclei of arbitrary spin. The HYSCORE spectrum from nuclear spin I can be generally described by (*25*)

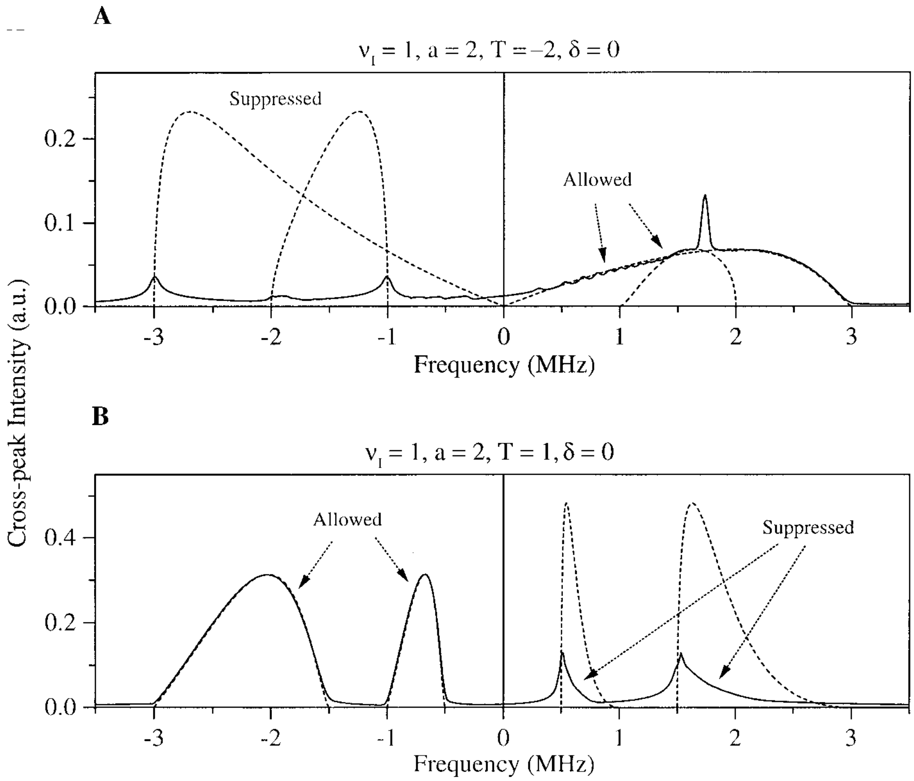

FIG. 8. Comparison of theoretical profiles for the powder cross-peaks calculated analytically using [10] (dashed lines) with sky-line profiles in simulated HYSCORE spectra (solid lines). The parameters were $I = 1/2$, $\nu_I = 1$ MHz, (A) $a = 2$ MHz, $T = -2$ MHz, (B) $a = 2$ MHz, $T = 1$ MHz. The positive frequency corresponds to cross-peak intensity in (+, +) quadrant and negative in (+, −) quadrant. The spike at 1.73 MHz in the intensity profile (A) is due to the intersection of the two cross-peak ridges.

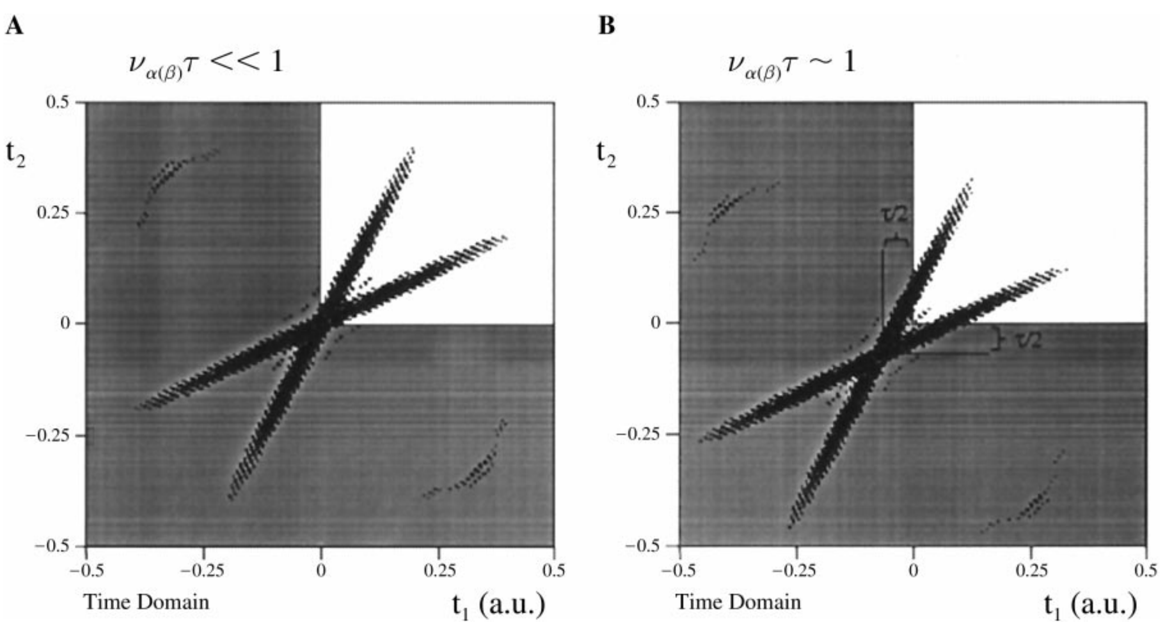

FIG. 9. The τ-shift effect in powder HYSCORE experiment. The two straight lines of maximum modulation signal ([14], [15], or [16]) are shifted to negative times on (B) to make an intersection at ($t_1 = -\tau/2$, $t_2 = -\tau/2$). Only the light area ($+t_1$, $+t_2$) is detectable in HYSCORE experiments.

$$V(t_1, t_2) \propto \left\langle \begin{array}{l} \Sigma_{i,j}\,(k_{i,j}e^{-i\cdot 2\pi(\nu_{\alpha i}t_1+\nu_{\beta j}t_2+(\nu_{\alpha i}+\nu_{\beta j})\tau/2)} \\ \quad + k^*_{i,j}e^{-i\cdot 2\pi(\nu_{\alpha i}t_2+\nu_{\beta j}t_1+(\nu_{\alpha i}+\nu_{\beta j})\tau/2)} + \text{c.c.} \\ \quad + (l_{i,j}e^{-i\cdot 2\pi(\nu_{\alpha i}t_1-\nu_{\beta j}t_2+(\nu_{\alpha i}-\nu_{\beta j})\tau/2)} \\ \quad + l^*_{i,j}e^{-i\cdot 2\pi(\nu_{\alpha i}t_2-\nu_{\beta j}t_1+(\nu_{\alpha i}-\nu_{\beta j})\tau/2)} + \text{c.c.} \end{array} \right\rangle_\Omega,$$

where the sum is taken over the different nuclear frequencies $\nu_{\alpha i}$ and $\nu_{\beta j}$ from opposite electron spin manifolds. In contrast to the $I = 1/2$ case [11], the amplitude coefficients $k_{i,j}(l_{i,j})$ are complex values with initial phases ph($k_{i,j}$) and ph($l_{i,j}$) which influence the time-domain signal:

$$\text{ph}(\Omega, t_1, t_2) = \nu_{\alpha i}(\Omega)t_1 + \nu_{\beta j}(\Omega)t_2 + (\nu_{\alpha i}(\Omega) + \nu_{\beta j}(\Omega))\tau/2 + \text{ph}(k(l)_{i,j}).$$

In the linear segment approximation, $\nu_{\alpha i}(\Omega) = b_1 \cdot \nu_{\beta j}(\Omega) + b_0$, the time-domain signals have the same phase at

$$b_1t_1 + t_2 + (b_1 + 1)\tau/2 + \text{ph}(k(l)_{i,j})/\nu_\beta(\Omega) = 0. \qquad [19]$$

which differs from the $I = 1/2$ case [14] by $\text{ph}(k(l)_{i,j})/\nu_\beta(\Omega)$. The latter term is orientation dependent and therefore the location the observable time-domain signals is not obvious. It is clear, however, that this term becomes negligible at larger times $t_{1(2)}$ so that [19] approaches the straight line, $b_1t_1 + t_2 + \text{const} = 0$, similar to [14]. Therefore, one would expect that the lines of maximum intensity in the time domain are located in the same manner as in the $I = 1/2$ case and the same qualitative description of interference effects should apply in the frequency domain (see Table 1). Numerical simulations and experimental HYSCORE spectra from $I = 1$ (*3, 9, 13*), 3/2 (*14, 15*), and 5/2 (*7*) nuclei support this qualitative conclusion.

Cross-Peak Intensity in the Case of Nonaxial HFI

Nuclear frequencies for a nonaxial hyperfine interaction depend on the polar (θ) and azimuthal (φ) angles that relate the magnetic field orientation to the HFI principal axis system,

$$\begin{aligned} \nu^2_{\alpha(\beta)} &= \nu^2_{z\alpha(\beta)}\cos^2\theta + \nu^2_{y\alpha(\beta)}\sin^2\theta\cdot\sin^2\varphi \\ &\quad + \nu^2_{x\alpha(\beta)}\sin^2\theta\cdot\cos^2\varphi \\ &= \nu^2_{z\alpha(\beta)}\cos^2\theta + \frac{\nu^2_{x\alpha(\beta)} + \nu^2_{y\alpha(\beta)}}{2}\cdot\sin^2\theta \\ &\quad + \frac{\nu^2_{x\alpha(\beta)} - \nu^2_{y\alpha(\beta)}}{2}\cdot\sin^2\theta\cdot\cos 2\varphi, \end{aligned} \qquad [20]$$

where $\nu_{z\alpha(\beta)} = -\nu_I \pm (a + 2T)/2$ and $\nu_{x(y)\alpha(\beta)} = -\nu_I \pm (a - T(1 \pm \delta))/2$ are nuclear frequencies at the canonical orientations of the HFI tensor $[-T(1 + \delta), -T(1 - \delta), +2T]$.

The general relation $S_{\nu_\alpha,\nu_\beta}\cdot d\nu_\alpha\cdot d\nu_\beta = I(\theta, \varphi)\cdot\sin\theta\cdot d\theta\cdot d\varphi$ for cross-peak intensity can be written using the Jacobian form,

$$S_{\nu_\alpha,\nu_\beta} = I(\theta, \varphi)\cdot\sin\theta\cdot\left|\frac{\partial(\theta, \varphi)}{\partial(\nu_\alpha, \nu_\beta)}\right|, \quad \text{with}$$

$$\left|\frac{\partial(\theta, \varphi)}{\partial(\nu_\alpha, \nu_\beta)}\right| = \begin{vmatrix} \dfrac{\partial\nu_\alpha}{\partial\theta} & \dfrac{\partial\nu_\beta}{\partial\theta} \\ \dfrac{\partial\nu_\alpha}{\partial\varphi} & \dfrac{\partial\nu_\beta}{\partial\varphi} \end{vmatrix}^{-1}.$$

Thus one obtains

$$S^\pm_{\nu_\alpha,\nu_\beta} = \frac{\nu_I\cdot z^2(\delta^2\sin^2 2\varphi + (3 + \delta\cos 2\varphi)^2\cos^2\theta)}{\delta\cdot T\cdot(9 - \delta^2)\cdot\nu_\alpha\nu_\beta\cdot\sin\varphi\cdot\cos\varphi\cdot\cos\theta} \times I_2(\nu_\alpha\tau, \nu_\beta\tau), \qquad [21]$$

where again the second term describes the blind-spot effect and is omitted in further discussion. There are apparent singularities in the cross-peak shape in Eq. [21]. They occur when one of the following conditions is met: $\sin\varphi = 0$, $\cos\varphi = 0$, or $\cos\theta = 0$, that is for the magnetic field perpendicular to a principal axis of the HFI tensor. The singularities can be easily understood from the second form of Eq. [20]. For those orientations with the same angle θ, both ν^2_α and ν^2_β vary as $\cos 2\varphi$. Thus, $\varphi = 0$ and $\varphi = \pi/2$ are stationary points for ν_α and ν_β so that many orientations have $\cos 2\varphi \approx \pm 1$ and contribute to spectral intensity at the extreme value of ν_α and ν_β, for that value of θ. Similar turning points occur along the entire length of each of the three boundary arcs for the cross-peak.

The powder cross-peaks have a horn shape for nonaxial HFI (*20*). The three arcs corresponding to $\sin\varphi = 0$, $\cos\varphi = 0$, and $\cos\theta = 0$ bound the range of possible frequencies for that HFI and are also the conditions for the singularities in Eq. [21]. Therefore, one expects the outlines to be the most intense features in the spectrum. The outlining arcs are described by Eq. [7] with a different definition for the $Q_{\alpha(\beta)}$ and $G_{\alpha(\beta)}$ parameters (Table 2).

Figure 10 shows two spectra, each simulated for one nucleus with nonaxial HFI tensor. As expected, the spectra are dominated by the three separate arcs outlining the entire horn shape of the powder cross-peak (shaded). A significant aspect of both spectra is the distribution of the arc ridges between the (+, +) and (+, −) quadrants. The powder interference effects result in only ridges with negative values for $Q^{zx}_{\alpha(\beta)}$, $Q^{zy}_{\alpha(\beta)}$, or $Q^{xy}_{\alpha(\beta)}$ (Table 2) appearing in the (+, +) quadrant and only ridges with positive values appearing in the (+, −) quadrant.

The intensity profile along each outlining cross-peak arc can be obtained from Eq. [21] by substituting $\sin\varphi = 0$, $\cos\varphi = 0$, or $\cos\theta = 0$. The singularity term is transformed from angular to frequency coordinates as

TABLE 2
Arc Shape and Intensity Profiles for the Outlining Arcs of Powder Cross-Peak in the Case of Nonaxial HFI in HYSCORE Spectra for $S = 1/2$, $I = 1/2$

Powder arc (singularity)	Arc shape, $\nu^2_{\alpha(\beta)} = Q_{\alpha(\beta)}\nu^2_{\beta(\alpha)} + G_{\alpha(\beta)}$		"Ideal" intensity profile along the arc, $I^{\pm}_{13}$ ($z^2 \equiv c^2(s^2)$ and defined in [2])
Axial HFI	$Q_{\alpha(\beta)} = -\dfrac{\nu_{\parallel\alpha(\beta)} + \nu_{\perp\alpha(\beta)}}{\nu_{\parallel\beta(\alpha)} + \nu_{\perp\beta(\alpha)}}$	$G_{\alpha(\beta)} = -2\nu_I \cdot \dfrac{\nu_{\parallel\alpha}\nu_{\perp\beta} + \nu_{\parallel\beta}\nu_{\perp\alpha}}{\nu_{\parallel\beta(\alpha)} + \nu_{\perp\beta(\alpha)}}$	$\dfrac{6\lvert T\rvert \cdot \nu_I^2 z^2 \cos\theta \cdot \sin^2\theta}{\nu_\alpha\nu_\beta\sqrt{(\nu_{\parallel\alpha} + \nu_{\perp\alpha})^2\nu_\beta^2 + (\nu^2_{\parallel\beta} + \nu^2_{\perp\beta})^2\nu^2_\alpha}}$, where $\nu^2_{\alpha(\beta)} = \nu^2_{\parallel\alpha(\beta)}\cos^2\theta + \nu^2_{\perp\alpha(\beta)}\sin^2\theta$
Nonaxial HFI			
ZX-plane ($\sin\varphi = 0$)	$Q^{zx}_{\alpha(\beta)} = -\dfrac{\nu_{z\alpha(\beta)} + \nu_{x\alpha(\beta)}}{\nu_{z\beta(\alpha)} + \nu_{x\beta(\alpha)}}$	$G^{zx}_{\alpha(\beta)} = -2\nu_I \cdot \dfrac{\nu_{z\alpha}\nu_{x\beta} + \nu_{z\beta}\nu_{x\alpha}}{\nu_{z\beta(\alpha)} + \nu_{x\beta(\alpha)}}$	$\dfrac{\nu_I^{3/2} \cdot z^2 \cdot \sin 2\theta}{\sqrt[4]{\nu^2_\alpha(\nu_{z\beta} + \nu_{x\beta})^2 + \nu^2_\beta(\nu_{z\alpha} + \nu_{x\alpha})^2}} \cdot \dfrac{3 + \delta}{\sqrt{4\delta(3 - \delta)}}$, where $\nu^2_{\alpha(\beta)} = \nu^2_{z\alpha(\beta)}\cos^2\theta + \nu^2_{x\alpha(\beta)}\sin^2\theta$
ZY-plane ($\cos\varphi = 0$)	$Q^{zy}_{\alpha(\beta)} = -\dfrac{\nu_{z\alpha(\beta)} + \nu_{y\alpha(\beta)}}{\nu_{z\beta(\alpha)} + \nu_{y\beta(\alpha)}}$	$G^{zy}_{\alpha(\beta)} = -2\nu_I \cdot \dfrac{\nu_{z\alpha}\nu_{y\beta} + \nu_{z\beta}\nu_{y\alpha}}{\nu_{z\beta(\alpha)} + \nu_{y\beta(\alpha)}}$	$\dfrac{\nu_I^{3/2} \cdot z^2 \cdot \sin 2\theta}{\sqrt[4]{\nu^2_\alpha(\nu_{z\beta} + \nu_{y\beta})^2 + \nu^2_\beta(\nu_{z\alpha} + \nu_{y\alpha})^2}} \cdot \dfrac{3 - \delta}{\sqrt{4\delta(3 + \delta)}}$, where $\nu^2_{\alpha(\beta)} = \nu^2_{z\alpha(\beta)}\cos^2\theta + \nu^2_{y\alpha(\beta)}\sin^2\theta$
XY-plane ($\cos\theta = 0$)	$Q^{xy}_{\alpha(\beta)} = -\dfrac{\nu_{x\alpha(\beta)} + \nu_{y\alpha(\beta)}}{\nu_{x\beta(\alpha)} + \nu_{y\beta(\alpha)}}$	$G^{xy}_{\alpha(\beta)} = -2\nu_I \cdot \dfrac{\nu_{x\alpha}\nu_{y\beta} + \nu_{x\beta}\nu_{y\alpha}}{\nu_{x\beta(\alpha)} + \nu_{y\beta(\alpha)}}$	$\dfrac{\nu_I^{3/2} \cdot z^2 \cdot \sin 2\varphi}{\sqrt[4]{\nu^2_\alpha(\nu_{x\beta} + \nu_{y\beta})^2 + \nu^2_\beta(\nu_{x\alpha} + \nu_{y\alpha})^2}} \cdot \dfrac{2\delta}{\sqrt{2(9 - \delta^2)}}$, where $\nu^2_{\alpha(\beta)} = \nu^2_{x\alpha(\beta)}\cos^2\varphi + \nu^2_{y\alpha(\beta)}\sin^2\varphi$

$$\frac{1}{|\sin\varphi|} = \frac{1}{\sqrt{\Delta\nu}} \cdot \frac{\sqrt{\nu_I\delta(3 - \delta)} \cdot T\sin\theta}{[(\nu_{z\beta} + \nu_{x\beta})^2\nu^2_\alpha + (\nu_{z\alpha} + \nu_{x\alpha})^2\nu^2_\beta]^{0.25}},$$
$$\frac{1}{|\cos\varphi|} = \frac{1}{\sqrt{\Delta\nu}} \cdot \frac{\sqrt{\nu_I\delta(3 + \delta)} \cdot T\sin\theta}{[(\nu_{z\beta} + \nu_{y\beta})^2\nu^2_\alpha + (\nu_{z\alpha} + \nu_{y\alpha})^2\nu^2_\beta]^{0.25}},$$
$$\frac{1}{|\cos\theta|} = \frac{1}{\sqrt{\Delta\nu}} \cdot \frac{\sqrt{\nu_I(9 - \delta^2)/2} \cdot T}{[(\nu_{x\beta} + \nu_{y\beta})^2\nu^2_\alpha + (\nu_{x\alpha} + \nu_{y\alpha})^2\nu^2_\beta]^{0.25}},$$
[22]

where $1/\sqrt{\Delta\nu}$ would result from integration of the square-root singularity when some homogeneous broadening of the individual spectral components is introduced; $\Delta\nu$ can vary across the spectrum depending on the precise nature of the broadening but will be assumed to be constant for the purpose of discussion. Substituting [22] into [21], one derives the intensity profiles along the length of the outlining ridges:

$$S^{\pm}_{\nu_\alpha,\nu_\beta} = \frac{1}{\sqrt{\Delta\nu}} \cdot I^{\pm}_{13}(\nu_\alpha, \nu_\beta; \nu_I, a, T, \delta) \times I_2(\nu_\alpha\tau, \nu_\beta\tau) \cdot I_4(Q_{\alpha(\beta)}), \quad [23]$$

where I_2 and I_4 are the blind-spot and interference terms, and $I^{\pm}_{13}$ is "true" intensity shape. The latter are collected in Table 2 for each of the outlining ridges.

All three edges have smooth shapes similar to those found for axial HFI [10]. The arc has a single maximum along its length and falls to zero at the canonical orientations. Because each of the outlining ridges has an intensity profile similar to that for the axial HFI case, which is described by Eq. [7], then one nonaxial nucleus produces a cross-peak pattern closely resembling what would result from three (nonequivalent) axial nuclei having principal values in common with each other. In addition, the powder interference effects will distribute each of the three outlining ridges between the two quadrants of the 2D spectra (Fig. 10) to further complicate interpretation. However, in a ν^2_α vs ν^2_β plot, the ridges become straight lines (*20*) and each pair of oulining ridges should intersect at $|\nu_\alpha \pm \nu_\beta| = 2\nu_I$. This is the most direct indication for the ridges produced by a single nucleus with nonaxial HFI.

We now consider the relative intensities of the three ridges of nonaxial cross-peaks. If the hyperfine interaction is weak ($\nu_I > |a|, |T|$), then $c^2 \approx 1$ and $s^2 \approx 0$ for all three ridges, and they appear mainly in the $(+, +)$ quadrant. The denominators in $I^{\pm}_{13}$ have roughly the same magnitude for all ridges. As a result, the relative intensities of the ridges are determined solely by the rhombic parameter:

$$S^{zx}:S^{zy}:S^{xy} = (3 + \delta)^{3/2}:(3 - \delta)^{3/2}:(2\delta)^{3/2}, \quad [24]$$

and vary from 1:1:0 for nearly axial HFI ($\delta \approx 0$) to 2.8:1:1 for a purely rhombic hyperfine interaction ($\delta = 1$). The same ratios are obtained for the case of strong isotropic HFI coupling ($|a| > \nu_I, |T|$); however, all ridges appear in the $(+, -)$ quadrant ($c^2 \approx 0$ and $s^2 \approx 1$).

CONCLUSIONS

The analysis presented here extends the theoretical treatment of cross-peaks in powder HYSCORE spectra of $I = 1/2$ nucleus started previously (*12, 20*). Cross-peaks form well-defined ridges (arcs and horns) in 2D spectra which allow accurate estimation of isotropic and anisotropic hyperfine pa-

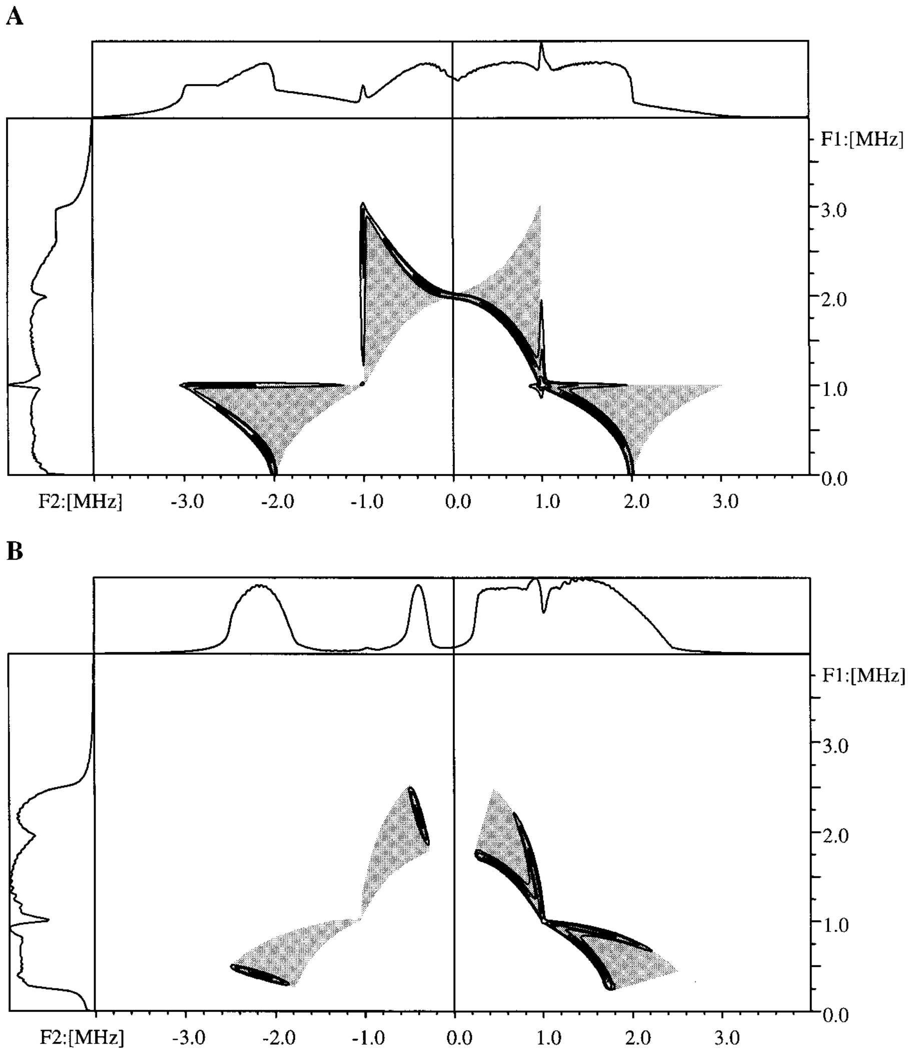

FIG. 10. Simulated powder HYSCORE spectra from an $I = 1/2$ with nonaxial HFI: (A) $\nu_I = 1$ MHz, $a = 2$ MHz, $T = -1$ MHz, $\delta = 1$, and (B) $\nu_I = 1$ MHz, $a = 1.5$ MHz, $T = -0.75$ MHz, $\delta = 1$.

rameters. In the present work we concentrate on the intensities and shapes of those ridges. A new feature of powder 2D spectra, the suppression of some ridges by interference effects, was discovered. Interference leads to suppression in one of the $(+, +)$ or $(+, -)$ quadrants of 2D spectra depending on the orientation of the cross-peak relative to the spectral axes. This is a fundamental difference with respect to single-crystal (oriented) systems where cross-peaks appear in both quadrants, determined solely by the ratio $c^2{:}s^2$. The intensity profile along the powder cross-peak, in the case of axial hyperfine interaction, is a bell-type shape with a single maximum and with zero intensity at the canonical ($\|$ and $\perp$) orientations of the magnetic field. Nonaxial hyperfine interaction produces three separate arc ridges corresponding to orientations of the magnetic field perpendicular to each of the principal axes of the nonaxial HFI tensor. Only these canonical ridges are observable in the spectra and outline the whole horn shapes predicted for nonaxial HFI. These ridges provide a convenient basis for rapidly evaluating the entire hyperfine tensor.

ACKNOWLEDGMENTS

Part of this work was performed at the Pacific Northwest National Laboratory, a multiprogram national laboratory operated by Battelle Memorial Institute for the U.S. Department of Energy under Contract DE-AC06-76RLO 1830. The William R. Wiley Environmental Molecular Sciences Laboratory is a national scientific user facility sponsored by the U.S. DOE's Office of Biological and Environmental Research and located at PNNL. Supported by office of Biological and Environmental Research, U.S. DOE. The research was also supported by Associated Western Universities, Inc., Northwest Division (AWU NW), under Grant DE-FG06-89ER-75522 or DE-FG06-92RL-12451 with the U.S. Department of Energy and by DOE/OBER. A.M.T. acknowledges the receipt of Postdoctoral Fellowships from the Associated Western Universities.

REFERENCES

1. P. Höfer, A. Grupp, H. Nebenführ, and M. Mehring, Hyperfine sublevel correlation (HYSCORE) spectroscopy: A 2D ESR investigation of the squaric acid radical, *Chem. Phys. Lett.* **132,** 279–283 (1986).
2. H. Käss, J. Rautter, B. Bönigk, P. Höfer, and W. Lubitz, 2D ESEEM of the ^{15}N-labeled radical cations of bacteriochlorophyll *a* and of the primary donor in reaction centers of *Rhodobacter sphaeroides, J. Phys. Chem.* **99,** 436–448 (1995).
3. S. A. Dikanov, R. I. Samoilova, J. A. Smieja, and M. K. Bowman, Two-dimensional ESEEM study of VO^{2+} complexes with imidazole and hystidine: Histidine is a polydentante ligand, *J. Am. Chem. Soc.* **117,** 10579–10580 (1995).
4. V. Kofman, O. Farver, I. Pecht, and D. Goldfarb, Two-dimensional pulsed EPR spectroscopy of the copper protein azurin, *J. Am. Chem. Soc.* **118,** 1201–1206 (1996).
5. D. Zhao, J. J. Shane, W. Daniel, P. G. Harrison, and D. Goldfarb, A pulsed EPR study of the catalytic oxidation of CO over Cu/SnO_2, *Appl. Magn. Reson.* **10,** 539–557 (1996).
6. A. Pöppl and L. Kevan, A practical strategy for determination of proton hyperfine interaction parameters in paramagnetic transition metal ion complexes by two-dimensional HYSCORE electron spin resonance spectroscopy in disordered systems, *J. Phys. Chem.* **100,** 3387–3394 (1996).
7. R. I. Samoilova, S. A. Dikanov, A. V. Fionov, A. M. Tyryshkin, E. V. Lunina, and M. K. Bowman, Pulsed EPR study of orthophosphoric and boric acid modified γ-alumina, *J. Phys. Chem.* **100,** 17621–17629 (1996).
8. Y. Deligiannakis and A. W. Rutherford, One- and two-dimensional electron spin echo envelope modulation study of the intermediate electron acceptor pheophytin in ^{14}N- and ^{15}N-labeled photosystem II, *J. Am. Chem. Soc.* **119,** 4471–4480 (1997).
9. P. J. van Dam, E. J. Reijerse, and W. R. Hagen, Identification of a putative histidine base and of a non-protein nitrogen ligand in the active site of Fe-hydrogenases by one-dimensional and two-dimensional electron spin-echo envelope-modulation spectroscopy, *Eur. J. Biochem.* **248,** 355–361 (1997).
10. P. M. Schosseler, B. Wehrli, and A. Schweiger, Complexation of copper(II) with carbonate ligands in aqueous solution: A CW and pulse EPR study, *Inorg. Chem.* **36,** 4490–4499 (1997).
11. J. I. Martinez, P. J. Alonso, C. Gómez-Moreno, and M. Medina, One- and two-dimensional ESEEM spectroscopy of flavoproteins, *Biochemistry* **36,** 15526–15537 (1997).
12. S. A. Dikanov and M. K. Bowman, Determination of ligand conformation in reduced [2Fe-2S] ferredoxin from cysteine β-proton hyperfine couplings, *J. Biol. Inorg. Chem.* **3,** 18–29 (1998).
13. S. A. Dikanov, R. M. Davydov, A. Gräslund, and M. K. Bowman, Two-dimensional ESEEM spectroscopy of nitrogen hyperfine couplings in methemerythrin and azidomethemerythrin, *J. Am. Chem. Soc.* **120,** 6797–6805 (1998).
14. Y. Deligiannakis, L. Astrakas, G. Kordas, and R. A. Smith, Electronic structure of B_2O_3 glass studied by one- and two-dimensional electron-spin-echo envelope modulation spectroscopy, *Phys. Rev. B* **58,** 11420–11434 (1998).
15. L. Astrakas, Y. Deligiannakis, G. Mitrikas, and G. Kordas, Hyperfine sublevel correlation spectroscopy in lithium silicate glasses, *J. Chem. Phys.* **109,** 8612–8616 (1998).
16. Y. Deligiannakis, J. Hanley, and A. W. Rutherford, 1D- and 2D-ESEEM study of the semiquinone radical Q_A^- of photosystem II, *J. Am. Chem. Soc.* **121,** 7653–7664 (1999).
17. D. G. Gilbert, S. A. Dikanov, D. C. Doetschman, and J. A. Smieja, A study of pyridil nytrosyl iron(II) tetraphenyl $^{15}N_4$-porphyrin. NO geometry and spin coupling to the pyrrole nitrogens, *Chem. Phys. Lett.* **315,** 43–48 (1999).
18. S. A. Dikanov, B. D. Liboiron, K. H. Thompson, E. Vera, V. G. Yuen, J. H. McNeil, and C. Orvig. In vivo electron spin-echo envelope modulation (ESEEM) spectroscopy: First observation of vanadyl coordination to phosphate in bone, *J. Am. Chem. Soc.* **121,** 11004–11005 (1999).
19. J. J. Shane, P. Höfer, E. J. Reijerse, and E. de Boer, Hyperfine sublevel correlation spectroscopy (HYSCORE) of disordered solids, *J. Magn. Reson.* **99,** 596–604 (1992).
20. S. A. Dikanov and M. K. Bowman, Cross-peak lineshape of two-dimensional ESEEM spectra in disordered $S = 1/2$, $I = 1/2$ spin systems, *J. Magn. Reson. A* **116,** 125–128 (1995).
21. C. Gemperle, G. Aebli, A. Schweiger, and R. R. Ernst, Phase cycling in pulsed EPR, *J. Magn. Reson.* **88,** 241–256 (1990).
22. A. M. Tyryshkin, S. A. Dikanov, and D. Goldfarb, Sum combination harmonics in four-pulse ESEEM spectra. Study of the ligand geometry in aqua–vanadyl complexes in polycrystalline and glass matrices, *J. Magn. Reson. A* **105,** 271–283 (1993).
23. P. Höfer, Distortion-free electron-spin-echo envelope-modulation spectra of disordered solids obtained from two- and three-dimensional HYSCORE spectra, *J. Magn. Reson. A* **111,** 77–86 (1994).
24. A. V. Astashkin, S. A. Dikanov, and Yu. D. Tsvetkov, Spectrometer dead time: Effect on electron spin echo modulation spectra in disordered systems, *Chem. Phys. Lett.* **136,** 204–209 (1987).
25. J. J. Shane, Electron spin echo envelope modulation spectroscopy of disordered solids, Ph.D. thesis, Catholic University of Nijmegen, The Netherlands, p. 67 (1993).